

TWELFTH EUROPEAN ROTORCRAFT FORUM

Paper No. 22

A PARAMETRIC INVESTIGATION OF A FREE WAKE  
ANALYSIS OF HOVERING ROTORS

A. Graber and A. Rosen

Department of Aeronautical Engineering  
Technion - Israel Institute of Technology  
Haifa, Israel

September 22-25, 1986

Garmisch-Partenkirchen  
Federal Republic of Germany

Deutsche Gesellschaft für Luft- und Raumfahrt e. V. (DGLR)  
Godesberger Allee 70, D-5300 Bonn 2, F.R.G

# A PARAMETRIC INVESTIGATION OF A FREE WAKE ANALYSIS OF HOVERING ROTORS

A. Graber\* and A. Rosen\*\*  
Department of Aeronautical Engineering  
Technion-Israel Institute of Technology  
Haifa, Israel

## ABSTRACT

A recently developed free wake model of a hovering rotor is used in order to perform a study of the influence of different parameters on the accuracy and efficiency of the calculations. The parameters that will be investigated include: the spanwise and chordwise distribution of cells over the blade, the length of the near wake, the length of the straight vortex elements of which the near wake is assembled, the vortex core size, relaxation factors and the influence of including a correction for the self induction in the near wake due to the curvature of the real trailing vortex elements. This parametric investigation is aimed at giving future users of free wake analyses guidelines on how to arrive at a numerical model which is accurate and still efficient. The last part of the paper will include a free wake analysis of a rotor having swept blades in order to learn about the influence of the sweep back on the aerodynamic behavior.

## 1. Introduction

Free wake analysis of helicopters' rotors is a very important tool to investigate their aerodynamic behavior. While prescribed wake models usually give satisfactory results in forward flight, this is not true for hovering rotors. In this case the wake stays close to the rotor and large distances of wake have a significant influence on the aerodynamic behavior. This is especially true in the case of heavily loaded rotors where the use of prescribed wake models may yield poor predictions of the aerodynamic behavior. References 1-5 are representative examples of free wake investigations of rotors. A more detailed list of references may be found in Ref. 4.

While being a useful tool, free wake analyses on the other hand are very demanding when computer resources are considered. This includes both: computing time and memory size. The computing time required for a converged solution of one case is usually measured in CPU hours. The required computer resources is of course a function of the details of the model. Refinement of the blade or the wake description leads to a significant increase of the required computing time and memory size. Therefore it is not surprising that aerodynamicists are always trying to find the delicate balance between accuracy and efficiency.

The purpose of the present paper is to present a parametric study of the influences of different parameters (that define the numerical model details) on the accuracy of the results on one hand, and the

---

\*Graduate Student  
\*\*Associate Professor

computing time on the other. These results may assist future users of free wake analyses of rotors in deciding what will be the parameters they are going to use.

The models that have been developed in the past, by different investigators, present many differences among themselves. This may lead someone to wonder if a parametric study, using a certain model, maybe of any help to somebody who is going to use a different model. Fortunately the answer is positive. Although there may be differences between the models, they usually have important basic features in common. These common features include for example: the lifting surface is divided into cells in the spanwise and chordwise directions, the wake behind the blades is divided into different regions (near wake, far wake etc.), the accuracy of the wake description is determined by the number of trailing vortex filaments behind the blade and the length of the vortex elements along these filaments - and other common features. This paper will present a study of the influence of the basic features which are common to most of the free wake analyses that have been reported previously.

The model that will be used for the present parametric study is described in detail in Refs. 4, 5. In the next section a brief description of the model will be presented for the readers' convenience.

The parametric study will include three different rotors having straight blades (Refs. 6-8). In all cases the rotors are relatively heavily loaded and thus presenting the region where a free wake analysis is especially important. Moreover, one of the cases includes a four bladed rotor (most of the cases that have been reported in the past included two bladed rotors). Since most of the modern rotors include four or more blades - this four bladed rotor is interesting from a practical point of view.

The rotors that will be analysed have been chosen because experimental data already exist for them. This data includes in most of the cases the spanwise distribution of the aerodynamic loads along the blade and the geometry of the tip vortex. Thus almost a complete comparison between theory and experiment will be available. This comparison will help in assessing the quality of the theoretical results.

The present numerical model is capable of dealing with any geometry of the blade. This is very important nowadays since modern rotors have swept tips or different nonuniform planforms of the tips. The last part of the paper will present a free-wake analysis of the influence of sweep back on the aerodynamic behavior of the blade. This will include both: the distribution of aerodynamic loads along the blade and the geometry of the wake.

## 2. Brief Description of the Model and Solution Procedure

As already mentioned above, the model and solution procedure are described in detail in Refs. 4, 5. Here only a brief description for the readers convenience is presented.

The model is based on the Vortex Lattice Method (VLM) which is widely used in the free wake analysis of fixed wings. Each blade is divided into cells, as shown in Fig. 1. Since the largest aerodynamic loads appear at the tip region, and since very drastic variations of these loads occur there, the number of cells is usually increased towards the tip. As can be seen in Fig. 1 this increase in the number of cells includes both: reducing the width of the cells and increasing the number of cells in the chordwise direction. The geometry of the cells will be described by the blades' cross sections that define their left and right boundaries, and by indicating the chordwise division of cells at each column of cells.

The vorticity over the cell is concentrated on a horseshoe line vortex. This horseshoe is composed of a line vortex along the cell's quarter chord points and two bound trailing vortex filaments on both sides. At the mid span of the cell, at the three quarters chord point, a control point is located. At this point the condition of nonpenetration of the flow (tangency to the surface of the resultant velocity) is applied.

Trailing vortex filaments leave the blades and form the wake. The number of the trailing vortex filaments behind every blade is  $n$ , where  $(n-1)$  is the number of columns of cells along the blade. The vortex filaments are numbered from left (root) to right (tip). The circulation of these vortex filaments is constant and denoted  $\Gamma(1)$ ,  $\Gamma(2)$ ..,  $\Gamma(n)$  (see Fig. 1). Any point along the line is defined by its polar coordinates:  $r$ ,  $\varphi$ ,  $z$  (see Fig. 2). The azimuthal location,  $\varphi$ , is the only independent variable that doesn't change during the solution procedure. The radial distance  $r$  and the axial distance  $z$  are calculated during the solution procedure.  $x, y, r$  and  $z$  are non-dimensional coordinates. The appropriate dimensional coordinates are obtained after multiplication by the total length of the blade. This length is equal to  $R$  (the rip radius) in the case of straight blades.

The wake is divided into near and far wake regions. The near wake starts at the trailing edge of all the blades and ends at a certain azimuthal distance behind it. In Fig. 2 the  $j$ th vortex filament is shown. In the near wake region this filament is composed of straight vortex elements. The boundary points of these elements are denoted  $(1,j)$ ,  $(2,j)$ ... $(m(j),j)$ .  $m(j)$  is the last point in the near wake region. As indicated previously, while the azimuthal location of every point does not change during the solution procedure, the radial and axial locations  $(r(i,j)$  and  $z(i,j)$ , respectively) are calculated during the solution procedure.

It is known that curved vortex filaments induce velocities on themselves. A very important contribution to the self induction at a certain point of the curved element comes from other points in the neighborhood. This contribution disappears when the curved vortex filaments are approximated as a chain of straight elements. Therefore a correction is introduced in order to take account of the last contribution. This correction is similar to the one suggested in Ref. 9. A circular arc is fitted to every consecutive triad of points along the trailing vortex filaments. The vortex filament segment that includes the three points is approximated as a segment of a

ring. The self induced velocity at the mid-point is obtained by subtracting from the self induced velocity of the ring the contribution of the part of the ring that does not include the segment itself.

The far wake starts at the end of the near wake and is composed of semi-infinite helical vortex lines. The radius of this helix is equal to the radial location of the last point in the near wake,  $r(m(j),j)$ . The pitch of the helix,  $p(j)$ , is determined by the axial velocity which is induced at the last point of the vortex filament, at the near wake region. Thus it is clear that changes in the geometry of the near wake result in changes in the geometry of the far wake. The velocity which is induced by the semi-infinite helical vortex filaments along the blades and at all the points of the near wake, is calculated by applying a recently developed efficient method which is described in detail in Ref. 10. This method is a combination of numerical and analytical integrations.

In order to avoid singularity problems a vortex core model is used. Two vortex core models have been applied in Refs. 4, 5. One is the classical model of Rankine and the other is a continuous model that has been suggested by Sully<sup>9</sup>. It should be pointed out that besides solving the singularity problem, the vortex core model is not intended to present additional physical phenomena like vortex core bursting<sup>11</sup> or a non-penetration condition at the lifting surface<sup>12</sup>.

The solution procedure is presented in the block diagram shown in Fig. 3.

First, all the data concerning the: rotor geometry, angular velocity, air-density, cell distribution over the blade, the length of the near wake, number of vortex elements in the near wake, vortex core-size, and relaxation factors is read. Then initial values of the circulation distribution are obtained. These values may be obtained by using other theories (for example a prescribed wake model or a blade - element/momentum model), or using empirical data. Similarly an initial geometry of the wake is assumed. This geometry may consist of semi-infinite helical vortex filaments that start at the trailing edge of the blade, or a deformed helical structure based on empirical data.

Now the velocities which are induced at the near wake points, by all the elements of the flow field, are calculated. Knowing these velocities, a new near wake geometry is obtained by applying the condition that the wake is force-free. After the geometry of the near wake is updated, the geometry of the far wake is also updated based on the conditions at the end points of the near wake.

Based on the new geometry, the boundary conditions of non-penetration of the flow at the control points are applied. This yields a system of linear equations in the circulation strength of every cell. Solution of these equations yields the new vortex distribution.

At this stage the convergence of the solution is checked. This check may include the vortex distribution and geometry of the wake.

It may be either an automatic check or interactive. If convergence is not satisfied, a new iteration is started up by computing the induced velocities over the near wake.

In order to avoid oscillations during the iterative solution procedure, relaxation factors are applied. This means that the new geometry is chosen at some point between the "old" geometry and the one which is obtained by direct application of the condition of a force-free wake (for more details see Refs. 4,5). After convergence, the aerodynamic loads are calculated by applying the Kutta-Jukowski law.

The parametric study will include investigation of the influence of:

- . the length of the near wake
- . the number of cells and their distribution over the blade
- . the angular length of the elements in near wake
- . the vortex core size
- . the relaxation factor
- . self induced velocities due to curvature.

### 3. Details of the Parametric Investigation

#### 3.1 Rotors Analysed in the Investigation

As indicated above three different rotors are treated during the investigation. The details of the rotors are given in Table 1. These rotors are identical to those reported in Refs. 5-7, where experimental data is also provided.

Table 1: Details of the Three Rotors

rotor No.	1	2	3
reference number	5	6	7
number of blades	2	4	2
radius [m]	1.1430	0.75	1.05
chord [m]	0.1905	0.05	0.0762
solidity $\sigma$	0.106	0.0849	0.0462
aspect ratio	6	15	13.78
root cut out/radius	NA	0.22	0.134
the pitch angle at the root [degrees]	8	16.2	17.8
washout angle (pretwist) [degrees]	0	-8.3	-10.7
coning [degrees]	NA	2.5	1.5
$C_T/\sigma$	0.0433	0.0919	0.099
tip velocity [m/sec]	150	107	76.6

The rotors will be referred to in what follows according to their number - 1,2,3. Unlike the others, rotor 2 has four blades, which is the number of blades in many of the modern rotors. This rotor (No. 2) also presents a solidity typical of modern rotors while the

solidity of rotor No. 1 is relatively high and that of rotor No. 3 relatively low. The aspect ratio shows similar trends to the solidity. The root cut out of rotor No. 1 is not available and will be estimated as 0.2 of the rotor radius in the calculations. Error in this parameter should not have any important influence on the results. Rotors 2 and 3 have a linear washout (pretwist). The coning angle of rotor No. 1 is not available and therefore will be taken as zero in the calculations.

The thrust coefficients are relatively high, while rotor No. 2 exhibits the highest. The thrust coefficient of rotor 2 is calculated by using the data of Ref. 13.

The tip velocity in all three cases is relatively low so that compressibility effect are not important and can be neglected.

### 3.2 The Numerical Investigation

The numerical investigation includes a total of twenty-one numerical configurations - six configurations of rotor No. 1, eleven configurations of rotor No. 2 and four configurations of rotor No. 3. The configurations' details are given in Table 2.

Each of the numerical configurations will be referred to in what follows according to its number as it appears in the first column. The number of columns of cells is equal to  $(n-1)$  where (as indicated above)  $n$  is the number of trailing vortices behind each blade. The present investigation includes only two different divisions into columns of cells. The first one includes eight columns which are defined by the following cross sections:  $x=x_r$ , 0.4, 0.6, 0.7, 0.8, 0.85, 0.9, 0.95, 1.0 ( $x_r$  is the root cut out cross section). The second division includes twelve columns, defined by the following cross sections:  $x=x_r$ , 0.35, 0.45, 0.55, 0.65, 0.75, 0.8, 0.85, 0.9, 0.925, 0.95, 0.975, 1.0. Each column may have a different number of cells in the chordwise direction. In the present investigation the chordwise division of any column is uniform. The number of chordwise cells runs between a single cell and up to four cells. There are four different kinds of distributions of cells which are denoted I, II, III and IV and are defined in Table 3. Configurations I and II have only one cell in every column (they have eight and twelve columns, respectively). Configurations III and IV exhibit an increasing number of cells per column, toward the tip.

The length of the near wake should be related to the number of blades. Previous investigations have indicated as an appropriate length an azimuthal length of two and a half times the azimuthal distance between neighboring blades. This means a near wake length of  $450^\circ$  and  $225^\circ$  for two and four bladed rotors, respectively. For rotors No. 1 and 2 the influence of using half or twice these distances, will be investigated.

Of prime interest is the azimuthal distance of the straight vortex elements that assemble the trailing vortices in the near wake region. This distance, while constant along a certain filament, may vary from one filament to the other. In Table 4 details of the six different combinations of elements' length are presented.

Table 2 - Details of the Numerical Configurations.

Config. No.	rotor No.	No. of cell columns	chord-wise div. of cells*	total No. of cells	near wake length [degrees]	near wake config.**	vortex core radius (% of rotor radius)	relaxation factor	average CPU time per iteration [sec]‡
1A	1	8	III	17	450	$\alpha$	0.8	0.5	210
1B	1	8	III	17	900	$\alpha$	0.8	0.5	420
1C	1	8	III	17	225	$\alpha$	0.8	0.5	160
1D	1	8	I	8	450	$\alpha$	0.8	0.5	200
1E	1	12	II	12	450	$\tau$	0.8	0.5	430
1F	1	8	III	17	450	$\alpha$	0.8	0.8	200
2A	2	12	II	12	225	$\beta$	0.8	0.5	560
2B	2	12	IV	27	225	$\beta$	0.8	0.5	590
2C	2	12	II	12	225	$\beta$	0.4	0.5	560
2D	2	12	II	12	225	$\beta$	1.6	0.3	570
2E	2	8	I	8	225	$\gamma$	0.8	0.5	230
2F	2	8	I	8	112.5	$\gamma$	0.8	0.5	160
2G	2	8	I	8	225	$\gamma$	0.8	0.8	240
2H	2	8	I	8	450	$\gamma$	0.8	0.5	410
2I	2	12	II	12	225	$\delta$	0.8	0.5	310
2J	2	12	II	12	225	$\epsilon$	0.8	0.5	1000
2K	2	12	II	12	315	$\beta$	0.8	0.5	720
3A	3	8	I	8	450	$\gamma$	0.8	0.5	230
3B	3	8	I	8	450	$\gamma$	1.6	0.5	230
3C	3	8	I	8	450	$\gamma$	0.8	0.8	230
3D***	3	8	I	8	450	$\gamma$	0.8	0.5	220

\*see Table 3, \*\*see Table 4, \*\*\*without the self induction correction  
 ‡I.B.M. 308ID

Table 3 - The Chordwise Distribution of Cells.

config. \ column no.	column no.											
	1	2	3	4	5	6	7	8	9	10	11	12
I	1	1	1	1	1	1	1	1	-	-	-	-
II	1	1	1	1	1	1	1	1	1	1	1	1
III	1	1	1	2	2	3	3	4	-	-	-	-
IV	1	1	1	1	2	2	2	3	3	3	4	4

Table 4 - The Azimuthal Length of Vortex Elements in the Near Wake [degrees].

config. \ trailing vortex no.	trailing vortex no.												
	1	2	3	4	5	6	7	8	9	10	11	12	13
$\alpha$	32	32	28	25	22.5	20	19	17	16	15	-	-	-
$\beta$	25	25	22.5	20	19	17	16	15	14	13	14	13	13
$\gamma$	25	22.5	20	19	17	16	15	14	13	-	-	-	-
$\delta$	56	56	45	45	37.5	37.5	32	32	28	28	28	25	25
$\epsilon$	12.5	12.5	11	10	9	8.5	8	7.5	7.5	7	7	6.5	6.5
$\tau$	32	32	32	28	25	22.5	20	19	19	17	17	16	16

The vortex core model which will be used in the investigation is the classical Rankine model. In most of the cases (see Table 2) the vortex core radius is taken as 0.8% of the rotor radius. In order to check the influence of this parameter, results of taking values of 0.4% and 1.6% will also be presented.

The relaxation factor refers to the way in which the geometry of the new wake is determined. A relaxation factor of 0.5 indicates that the position of every point of the new wake is taken as the average between its "old" location and the location which is obtained by applying the condition that the wake should be free of forces (for more details see Refs. 4, 5). A value of 0.5 will be chosen in most of the cases. Few cases will have a relaxation factor of 0.8 which means that the new geometry is closer to that obtained by the free wake condition (the contributions to the new geometry include 80% of the geometry obtained by the free wake condition and 20% of the "old" geometry). All the configurations, except 3D, include corrections for self induction.

### 3.3 The Method of Presenting the Results

The calculations of the different configurations were carried out until convergence of the load distribution was obtained. In all the cases, except configurations 1B and 2H (long near wake), convergence of the wake geometry is also achieved. The average time per iteration is given in Table 2. Few improvements in the numerical procedures have helped in reducing the time compared to what had been reported in Refs. 4, 5.

The results that will be presented and discussed are of two kinds: the aerodynamic load distribution along the blade and the wake geometry.

The aerodynamic load distribution will be given as: lift coefficient, circulation or section loading distribution. Usually the same parameter that was measured experimentally, will be presented.

The wake geometry will specifically deal with the tip vortex geometry. In the calculations, in order to account for the wake roll-up, the "rolled-up" tip vortex location is defined as the "center of mass" of the three outer trailing vortices. Thus the equations describing this location are:

$$r_{tu} = \frac{\sum_{j=(n-2)}^n r_j \Gamma_j}{\sum_{j=(n-2)}^n |\Gamma_j|} ; z_{tu} = \frac{\sum_{j=(n-2)}^n z_j \Gamma_j}{\sum_{j=(n-2)}^n |\Gamma_j|}$$

$r_{tu}$ ,  $z_{tu}$  are the radial and axial nondimensional coordinates of the rolled-up tip vortex, respectively.

Usually the circulation  $\Gamma_n$  is much greater than  $\Gamma_{(n-1)}$  and  $\Gamma_{(n-2)}$ . Therefore the "rolled-up" tip vortex location is mainly determined by the geometry of the  $n$ th vortex line.

Experimental results for the tip vortex geometry exist for rotors Nos. 1 and 2, but not for rotor No. 3.

#### 4. Results and Discussion of the Parametric Study

The parametric study will be presented according to the different parameters which are investigated. While discussing a specific parameter, results of different rotors will be compared. Since experimental results of the wake geometry are not available for rotor no. 3, in most of the cases the comparison will be restricted to rotors nos. 1 and 2.

##### 4.1 The Near Wake Length

The influence of the length of the near wake, in the case of rotor no. 1, is shown in Figs. 4a,b. The standard near wake length (a length of two and a half spacings between blades) is  $450^\circ$  (configuration 1A). It is compared with a longer near wake ( $900^\circ$ , configuration 1B) and a shorter one ( $225^\circ$ , configuration 1C). It is shown in Fig. 4a that the spanwise lift coefficient distributions of the standard and long wake are very close. The short wake exhibits lower lift coefficients at the inner sections of the blade and thus shows better agreement with the experimental results.

The geometry of the tip vortex is shown in Fig. 4b. The standard wake exhibits nice agreement with the experimental results. The influence of the passage of the follower blade (after  $180^\circ$ ) is clearly seen in the theoretical and experimental results. The short wake exhibits nice agreement in its axial position, but the contraction is too strong. The long wake is very problematic from a numerical point of view. Not only that each iteration requires a longer computing time (approximately twice the standard model), but the convergence of the wake is slow and problematic and therefore will require a large number of iterations. The calculations of configuration 1B started from an initial cylindrical geometry. The results presented in the figure are those of the twenty-fifth iteration. The wavy nature of the tip vortex location indicates that convergence has not been reached yet, and more iterations will be required for proper convergence.

Figures 5a,b present the influence of the near wake length on rotor no. 2. Again, there is the standard length (configuration 2E,  $225^\circ$ ), longer near wake (configuration 2H,  $450^\circ$ ) and a shorter one (configuration 2F,  $112.5^\circ$ ). The spanwise distribution of the circulation is presented in Fig. 5a. At the tip region the standard and short wake practically give identical results, while the long wake results are higher. At the inner sections the results of the short and long near wakes are higher than the standard model. The shorter near wake gives better agreement with the experiment at the inner cross-sections, while the longer near wake agrees better with the experimental results throughout the whole length. It should be noted that in the present calculations the pitch angle of the blades is taken as the value given in the experimental data. There is no increase of the pitch angle during the calculations in order to match the theoretical thrust coefficient with the experimental value (as was done for example in the calculations of Ref. 13).

The tip vortex geometry is described in Fig. 5b. The agreement with the experimental results of the axial location is good for all the configurations. The sudden increase in the axial induced velocity as a result of the passage of the follower blade (at an azimuth of ninety degrees) is clearly seen. In the case of the long near wake, a much smaller influence of the passage of the second follower blade (one hundred and eighty degrees) can also be seen. The main difference between the configurations appear in the radial location of the tip vortex. The short near wake is too short to predict the actual contraction (recall that the radius of the last point of the near wake becomes the radius of the semi-infinite helical vortex line). The standard wake seems to be the best in describing the contraction. After the passage of the follower blade the experimental results exhibit a significant decrease in the rate of contraction and the last points show a tendency to approach asymptotically a constant value of contraction. The standard model presents a decrease in the rate of contraction, similar to the experimental results, but still the theoretical rate is larger than that shown by the experimental points. The long near wake also shows a reduction in the contraction rate as a result of the passage of the follower blade. But this reduced rate is much higher than the experimental rate, and does not show a tendency to approach asymptotically a constant value of contraction during the first revolution. Therefore, because of the longer near wake, the contraction of the wake is much larger than in the case of the other configurations. This is probably the reason for the increase in the aerodynamic loads (of this configuration) at the tip region of the blade (see Fig. 5a). Similar to the case of rotor no. 1 the long near wake has not converged yet (at the twenty-fifth iteration) and the convergence procedure is slow and tends to be unstable. The results of rotor no. 2 indicate that it is possible that a near wake of  $225^\circ$  for a four bladed rotor may be too short to yield the correct contraction. On the other hand a wake of  $450^\circ$  fails to predict correctly the asymptotic approach to a constant contraction after the passage of the follower blade. In addition a near wake of  $450^\circ$  is very unstable and exhibits convergence difficulties. In order to clarify this point, further numerical investigation is required together with experimental measurements of the tip vortex geometry along longer distances (see additional results in the conclusions).

#### 4.2 The Number of Cells in the Chordwise Direction

Figure 6 shows the influence of increasing the number of chordwise cells in the tip region, on the lift coefficient distribution along the blades of rotor no. 1. The standard configuration (1A) has a total of seventeen cells increasing from one chordwise cell at the root region to four chordwise cells at the tip. The standard configuration is compared with configuration 1D having only one cell in the chordwise direction (over the whole length). As can be seen, the differences between both cases are negligible. The wake geometry is not presented since practically both configurations yield identical results. It should be noted that the blades of rotor no. 1 have a low aspect ratio and therefore these results are not fully expected.

Experimental results for the tip vortex geometry exist for rotors Nos. 1 and 2, but not for rotor No. 3.

#### 4. Results and Discussion of the Parametric Study

The parametric study will be presented according to the different parameters which are investigated. While discussing a specific parameter, results of different rotors will be compared. Since experimental results of the wake geometry are not available for rotor no. 3, in most of the cases the comparison will be restricted to rotors nos. 1 and 2.

##### 4.1 The Near Wake Length

The influence of the length of the near wake, in the case of rotor no. 1, is shown in Figs. 4a,b. The standard near wake length (a length of two and a half spacings between blades) is  $450^\circ$  (configuration 1A). It is compared with a longer near wake ( $900^\circ$ , configuration 1B) and a shorter one ( $225^\circ$ , configuration 1C). It is shown in Fig. 4a that the spanwise lift coefficient distributions of the standard and long wake are very close. The short wake exhibits lower lift coefficients at the inner sections of the blade and thus shows better agreement with the experimental results.

The geometry of the tip vortex is shown in Fig. 4b. The standard wake exhibits nice agreement with the experimental results. The influence of the passage of the follower blade (after  $180^\circ$ ) is clearly seen in the theoretical and experimental results. The short wake exhibits nice agreement in its axial position, but the contraction is too strong. The long wake is very problematic from a numerical point of view. Not only that each iteration requires a longer computing time (approximately twice the standard model), but the convergence of the wake is slow and problematic and therefore will require a large number of iterations. The calculations of configuration 1B started from an initial cylindrical geometry. The results presented in the figure are those of the twenty-fifth iteration. The wavy nature of the tip vortex location indicates that convergence has not been reached yet, and more iterations will be required for proper convergence.

Figures 5a,b present the influence of the near wake length on rotor no. 2. Again, there is the standard length (configuration 2E,  $225^\circ$ ), longer near wake (configuration 2H,  $450^\circ$ ) and a shorter one (configuration 2F,  $112.5^\circ$ ). The spanwise distribution of the circulation is presented in Fig. 5a. At the tip region the standard and short wake practically give identical results, while the long wake results are higher. At the inner sections the results of the short and long near wakes are higher than the standard model. The shorter near wake gives better agreement with the experiment at the inner cross-sections, while the longer near wake agrees better with the experimental results throughout the whole length. It should be noted that in the present calculations the pitch angle of the blades is taken as the value given in the experimental data. There is no increase of the pitch angle during the calculations in order to match the theoretical thrust coefficient with the experimental value (as was done for example in the calculations of Ref. 13).

The tip vortex geometry is described in Fig. 5b. The agreement with the experimental results of the axial location is good for all the configurations. The sudden increase in the axial induced velocity as a result of the passage of the follower blade (at an azimuth of ninety degrees) is clearly seen. In the case of the long near wake, a much smaller influence of the passage of the second follower blade (one hundred and eighty degrees) can also be seen. The main difference between the configurations appear in the radial location of the tip vortex. The short near wake is too short to predict the actual contraction (recall that the radius of the last point of the near wake becomes the radius of the semi-infinite helical vortex line). The standard wake seems to be the best in describing the contraction. After the passage of the follower blade the experimental results exhibit a significant decrease in the rate of contraction and the last points show a tendency to approach asymptotically a constant value of contraction. The standard model presents a decrease in the rate of contraction, similar to the experimental results, but still the theoretical rate is larger than that shown by the experimental points. The long near wake also shows a reduction in the contraction rate as a result of the passage of the follower blade. But this reduced rate is much higher than the experimental rate, and does not show a tendency to approach asymptotically a constant value of contraction during the first revolution. Therefore, because of the longer near wake, the contraction of the wake is much larger than in the case of the other configurations. This is probably the reason for the increase in the aerodynamic loads (of this configuration) at the tip region of the blade (see Fig. 5a). Similar to the case of rotor no. 1 the long near wake has not converged yet (at the twenty-fifth iteration) and the convergence procedure is slow and tends to be unstable. The results of rotor no. 2 indicate that it is possible that a near wake of  $225^\circ$  for a four bladed rotor may be too short to yield the correct contraction. On the other hand a wake of  $450^\circ$  fails to predict correctly the asymptotic approach to a constant contraction after the passage of the follower blade. In addition a near wake of  $450^\circ$  is very unstable and exhibits convergence difficulties. In order to clarify this point, further numerical investigation is required together with experimental measurements of the tip vortex geometry along longer distances (see additional results in the conclusions).

#### 4.2 The Number of Cells in the Chordwise Direction

Figure 6 shows the influence of increasing the number of chordwise cells in the tip region, on the lift coefficient distribution along the blades of rotor no. 1. The standard configuration (1A) has a total of seventeen cells increasing from one chordwise cell at the root region to four chordwise cells at the tip. The standard configuration is compared with configuration 1D having only one cell in the chordwise direction (over the whole length). As can be seen, the differences between both cases are negligible. The wake geometry is not presented since practically both configurations yield identical results. It should be noted that the blades of rotor no. 1 have a low aspect ratio and therefore these results are not fully expected.

Similar results are shown in Fig. 7 for rotor no. 2. The standard configuration 2A (with a single chordwise cell) is compared with configuration 2B having a total of twenty-seven cells. Only negligible differences appear at the tip region. Again the tip vortex geometry is identical in both cases and is not presented here.

In Fig. 8 the build up of the circulation, in the last column of cells of configuration 2B, is compared with the constant circulation of configuration 2A. As expected from Fig. 7 the value of the circulation leaving the trailing edge is practically identical in both cases.

As shown in Table 2, increasing the number of chordwise cells results in an insignificant increase of the average CPU time per iteration. This is due to the fact that the calculation of the new wake geometry (which consumes most of the computing time) is only very slightly influenced by an increase in the number of cells.

On the other hand it has been found in different cases that increasing the chordwise number of cells tends to stabilize the convergence procedure.

#### 4.3 The Spanwise Distribution of Columns of Cells

The spanwise distribution of columns of cells is important since it not only affects the accuracy of modelling the lifting surfaces, but it also determines the number of trailing vortex filaments. While investigating this point, configurations that include eight and twelve columns will be compared. The increase of "columns density" occurs mainly at the tip region.

In the case of rotor no. 1 configuration 1D includes eight columns while configuration 1E has twelve columns. Figure 9a shows that as a result of increasing the number of columns the lift coefficient is decreased, especially towards the root region. As a result the agreement with the experimental results is improved.

As shown in Fig. 9b the axial location of the tip vortex is only very slightly changed as a result of increasing the number of columns. The contraction on the other hand is decreased and the agreement with the experimental results is improved.

Similar trends also appear in the case of rotor no. 2. Figure 10a shows that as a result of increasing the number of columns, the circulation at the inner cross-sections is decreased and the peak at the tip becomes more pronounced. Concerning the tip vortex geometry, the configuration with twelve columns (2A) exhibits very nice agreement with the experimental results, while the configuration having only eight columns (2E) shows greater deviations.

The results of both rotors indicate that having twelve columns of cells seems to give good results. But at the same time the CPU time per iteration is increased significantly compared to eight columns.

#### 4.4 The Azimuthal Length of the Vortex Elements Composing the Near Wake

The azimuthal length of the elements in the near wake is considered as a very important parameter. Since small elements require a lot of computing time (see Table 2) the investigation will include only rotor no. 2. For the case of thirteen trailing vortex lines behind every blade, and a near wake length of  $225^\circ$ , three different configurations are compared. Configuration 2A is the standard one, having elements ranging from an azimuthal length of  $25^\circ$  at the root to  $13^\circ$  at the tip. Configuration 2I presents a coarser near wake where the length ranges between  $50^\circ$  and  $26^\circ$ . Configuration 2J includes the largest number of elements in the near wake, the length of which ranges between  $12.5^\circ$  and  $6.5^\circ$ .

Figure 11a presents the circulation distribution. Configurations 2A and 2I show similar behaviour where the coarser near wake (2I) exhibits slightly higher peak at the tip, and a lower minimum at the 0.85 spanwise station. Configuration 2J shows the smallest peak at the tip, and from the tip to the root (unlike the other configurations) there is a smooth decrease. It should be noted that this smooth decrease is in contrast to the experimental results that exhibit an increase in the circulation while going from cross-section 0.85 towards cross-section 0.75. This trend is also shown in the numerical results of configurations 2A and 2I.

The tip vortex geometry is presented in Fig. 11b. Concerning the axial location, configurations 2A and 2I agree very well between themselves and with the experimental results. Configuration 2J exhibits a larger axial velocity of the tip vortex. Concerning the radial location of the tip vortex the trends are different. In this case configurations 2A and 2J show nice agreement between themselves and with the experimental results. The coarse near wake (configuration 2I) yields a rate of contraction which is too large towards the end of the near wake. Thus it can be concluded that the standard near wake yields the best results concerning the tip vortex geometry.

It is also worth pointing out that configuration 2J, besides requiring a lot of computing time per iteration, also exhibits convergence and stability problems which makes it unattractive to use.

#### 4.5 The Vortex Core Radius

Figure 12 presents the influence of the vortex core radius on the spanwise circulation distribution, in the investigation of rotor no. 2. The standard configuration (2A) has a core radius of 0.8 percent of the rotor radius. Configuration 2C has a smaller core with a radius of 0.4 percent, while configuration 2D has a core radius of 1.6 percent of the rotor radius. It should be noted that all the vortex filaments, bound and free, have the same vortex core size.

The configurations having the standard core and the smaller one yield identical results. The configuration having the larger core (2D) gives higher circulation values at the tip region. The reason for this increase is that in this case the control points of the

cells at the tip are within the core region. Therefore the induced velocities at these points are decreased, causing an increase of the aerodynamic loads.

The tip vortex geometry is identical for the three configurations and therefore not presented here.

Similar results have also been obtained for rotor no. 3 (configurations 3A,3B).

The present results indicate that if a vortex core model is used in order to avoid singularity problems (and not to model physical phenomena as, for example, vortex bursting), then one should keep the core radius small enough in order to prevent influences of the core size on the results. On the other hand a too small radius may cause difficulties during the calculations.

#### 4.6 The Relaxation Factor

As indicated above, the relaxation factor is introduced in order to avoid instabilities during the iterative solution procedure. In order to investigate the influence of the magnitude of the relaxation factor, results for two values (0.5 and 0.8) will be presented.

Figure 13 presents the variation of the thrust coefficient with the iteration number, for rotor no. 2. Configuration 2E incorporates a relaxation factor of 0.5 while in configuration 2G the factor is 0.8. The initial wake geometry in all the present calculations is composed of semi-infinite helical vortex lines.

The case of using a higher relaxation factor exhibits a faster asymptotic convergence towards a value which is practically constant. After a small overshoot the tenth iteration presents in fact a converged solution. The convergence is much slower when a relaxation factor of 0.5 is used. Although the results in this case practically converge to the same value as in configuration 2G, they still show small oscillations after twenty-five iterations. As expected from the results of the spanwise distribution of loads, the value of the calculated thrust coefficient is lower than the experimental result (see the comment in subsection 4.1).

Figure 14 presents results for rotor no. 3. In this case the trends are completely different. Use of a relaxation factor of 0.5 exhibits a relatively nice convergence. From the second to the seventeenth iteration there is a very slow monotonic increase of the thrust coefficient. From the eighteenth to the twenty-third iteration there is a faster rate of increase, and then the calculated values remain almost constant and agree very well with the experimental value. Using a relaxation factor of 0.8 exhibits an increasing instability without a satisfactory convergence.

In Fig. 15 results for rotor no. 1 are presented. The trends are similar to the case of rotor no. 3. While the use of a relaxation factor of 0.5 shows relatively nice convergence, increasing instability is presented while applying a relaxation factor of 0.8.

The difference in the behavior while using a relaxation factor of 0.8, between rotor no. 2 and rotors nos. 1 and 3, may be a result of the differences in the near wake length. In the case of rotor no. 2 this length is 225° while in the two other cases it is 450°. This is also related to the number of blades. Further investigation is necessary in order to obtain a better insight into the nature of the influence of the relaxation factor. In the meantime it seems that a value of 0.5 is appropriate in most of the cases. Higher values of relaxation factors may give faster convergence, but they should be used with caution.

#### 4.7 Correction for Self Induction

The correction has been explained in the previous section. In Fig. 16 results for rotor no. 3, with (configuration 3A) and without (configuration 3D) self induction correction, are presented.

Figure 16a presents the spanwise circulation distribution. It is seen that the influence of the self induction is very small and practically negligible. The theoretical results agree very well with the experimental results.

The tip vortex geometry of both configurations is presented in Fig. 16b. Again the differences are very small.

#### 5. The Influence of Sweep Back

As indicated above the present model can deal with lifting surfaces having any planform. This capability will be used in order to investigate sweep influences. This investigation will include a comparison between a swept blade and a similar straight blade.

Rotor no. 3 is the basic rotor having straight blades. The swept blades are obtained (see Fig. 17a) by "cutting" the outer thirty percent of the blade and sweeping them back by 30°, relative to the other seventy percent. The planform of the swept part is identical to the same part of the straight blade (excluding for the sweep) except for the tip which is parallel to the y axis (the area of the straight and swept blade are identical). It is clear that cross-sections perpendicular to the axis of the swept portion will "see" a different flow field, even when induced velocities are not considered. Therefore in order to try and compare two rotors which are "similar to the maximum", the pitch angle of the cross-sections of the swept portion (the angle is measured about the swept axis) is changed. This angle is obtained by multiplying the pitch angle of the same cross-section of the straight blade by the factor f defined as:

$$f = \left[ \frac{\rho}{(\rho - \rho_s)} \frac{\sin \gamma}{\sin \Lambda} \frac{1}{\cos(\Lambda - \gamma)} \right]^2$$

where

$$\gamma = \arctan \frac{(\rho - \rho_s) \sin \Lambda}{\rho_s + (\rho - \rho_s) \cos \Lambda}$$

$r$  is a nondimensional coordinate along the blade axis, equal to zero at the root and one at the tip.  $r_s$  is the coordinate of the cross-section where the sweep back takes place and  $\Lambda$  the sweep angle there. It has been shown in Ref. 14 that based on a blade element theory, assuming identical induced velocity and neglecting small terms, both rotors will give identical aerodynamic loads. The division into cells is identical to the straight blade (configuration 3A) and shown in Fig. 17a as configuration SW1.

As can be seen from the circulation distribution along the blade (Fig. 17a), the load at the tip region is similar in both cases. On the other hand, at the sweep back region there is a significant influence which indicates that as a result of a sweep a trailing vortex filament appears which is much stronger than the trailing vortex leaving the same region of the straight blade. Because of this behavior it seems that at the sweep back region, a refinement of division of cells is desired. Configuration SW2 presents such a refinement (see Fig. 17a). It is seen that as a result of this refinement, shape change of the circulation at the sweep point is obtained. The intensity of the trailing vortex filament at this point is thirty percent of the strong tip vortex. Investigation of the wake (not seen here) reveals a roll-up phenomenon associated with this filament, similar to what happens in the case of the tip vortex.

The geometry of the tip vortex in the case of the three configurations is shown in Fig. 17b. The axial location is very similar in all the cases. There are some differences in the radial location. The decrease in the initial point is due to the fact that the radial location is normalized by the length of the blade (from rotor center to tip). In the case of the swept blade the length is larger than the radius of the tip. Besides these geometrical differences, it can be concluded that the radial location of the tip vortex is also similar in all the cases.

The present results indicate that sweep back introduces interesting phenomena in the aerodynamic behaviour of blades. Further investigation is required in order to get better insight into this influence.

## 6. Conclusions

Based on the parametric investigation presented in this paper, the following conclusions are drawn:

- Near wake length - for a two-bladed rotor a near wake length of  $450^\circ$  is appropriate. This length requires long computing time and tends to instability if appropriate relaxation factors are not applied. For a four-bladed rotor a near wake of  $225^\circ$  (or slightly longer) seems to give fair results. It has been shown that taking very long near wake increases the computing time significantly and introduces convergence difficulties.
- Number of cells in the chordwise direction - increasing the number of cells in the chordwise direction does not seem to change the results. On the other hand such an increase may

introduce better stability of the iterative computing procedure. Increasing the number of chordwise cells has only a mild influence on the required computing time.

- The spanwise distribution of columns of cells - twelve columns of cells, with increased number of columns at the tip region, seems to give good results for two- and four-bladed rotors. On the other hand it requires much more computing time compared to eight columns that offer results which in certain cases may be of sufficient quality.
- The azimuthal length of the vortex element of the near wake - a near wake composed of vortex elements ranging from an azimuthal length of  $25^\circ$  at the root to  $13^\circ$  at the tip, gives good results for two- and four-bladed rotors.
- The radius of the vortex core - in cases where the vortex core is introduced in order to avoid singularity problems, if it is kept small enough then it does not have influence on the results themselves.
- The relaxation factor - the relaxation factor is very important to the stability of the iterative procedure. A relaxation factor of 0.5 seems to be appropriate for a wide range of configurations. Higher relaxation factors may accelerate the convergence procedure, but on the other hand, they may cause instability of the iterative procedure. Therefore the use of higher relaxation factors requires special caution. The question of the optimal combination of relaxation factors (one may apply different relaxation factors to different parameters) still remains open and requires further investigation.
- Correction for self induction - has only a negligible influence on the results.
- Sweep back - as a result of sweep back of part of the blade, a relatively strong trailing vortex filament is formed at the sweep back region and the aerodynamic loads at this region are significantly changed, relative to a similar straight blade. A further investigation is required in order to get a better insight into the influences of sweep back.

The present study offers guidelines on how to choose a proper configuration for a free wake analysis of a certain rotor. Thus, for example, configuration no. 1E seems to be a good choice for a two-bladed rotor (see Figs. 9a,b). For a four-bladed rotor, configuration 2A seems appropriate. But based on the results of the present study, examination of a longer near wake is appealing. Thus configuration 2K has been calculated. The results are shown in Figs. 18a,b. As can be seen the longer near wake ( $315^\circ$ ) presents an improvement in the agreement with the experimental results. It is still up to the user to decide if the slight increase in the quality of the results are worth the large increase in CPU time. By examining the present results the aerodynamist has important information which helps him to find the delicate balance between accuracy and efficiency.

It is also worth mentioning, as indicated in Refs. 4,5, that the total required computing time may be dramatically reduced by starting the calculations from an initial wake geometry which is better than that composed of semi-infinite helical vortex filaments. This initial geometry may be obtained from calculations using simpler (and therefore cheaper to run) configuration, or using existing empirical data.

#### Acknowledgement

The authors would like to thank Mrs. A. Goodman-Pinto and Mrs. B. Hirsch for typing the paper and Mrs. E. Nitzan for the preparation of the figures.

#### References

1. D.R. Clark, A.C. Leiper            The Free Wake Analysis - a Method for the Prediction of Helicopter Rotor Hovering Performance  
J. of the American Helicopter Society (1970) 15 (1) 3-11.
2. H.F. Chou                            Helicopter Lifting Surface Theory with Force Free Wake  
West Virginia University Dept. of Aerospace Eng. Ph.D. Dissertation  
January 1975
3. L. Morino, Z. Kaprielian, S.R. Sipcic            Free Wake Analysis of Helicopter Rotors  
Paper No. 3 Ninth European Rotorcraft Forum Stresa Italy  
September 1983
4. A. Rosen, A. Graber                Free Wake Model of Hovering Rotors Having Straight or Curved Blades  
Proceedings of the International Conference on Rotorcraft Basic Research Research Triangle Park  
North Carolina February 1985
5. A. Rosen, A. Graber                Free Wake Model of Hovering Rotors Having Straight or Curved Blades  
Has been accepted for publication in the Journal of the American Helicopter Society (condensed version of Ref. 4)
6. F.X. Caradonna, C. Tung            Experimental and Analytical Studies of a Model Helicopter Rotor in Hover  
Vertica (1981) 5 149-161

7. D. Favier, M. Nsi Mba,  
C. Barbi, C. Maresca      A Free Wake Analysis for Hovering  
Rotors and Advancing Propellers  
Paper No. 21 Eleventh European  
Rotorcraft Forum London England  
September 1985
  
8. J.D. Ballard, K.L. Orloff,  
A. Luebs      Effect of Tip Shape on Blade  
Loading Characteristics and Wake  
Geometry for a Two Blades Rotor in  
Hover  
J. of the American Helicopter  
Society (1980) 25 30-35
  
9. M.P. Scully      Computation of Helicopter Rotor  
Wake Geometry and Its Influence on  
Rotor Harmonic Airloads  
M.I.T. Dept. of Aeronautical Eng.  
Ph.D. Dissertation February 1975
  
10. A. Graber, A. Rosen      Calculating the Axial and Radial  
Velocities Induced by Semi-  
Infinite Helical Vortex Lines  
Has been submitted for publication
  
11. R.H. Miller      Rotor Hovering Performance Using  
the Method of Fast Free Wake  
Analysis  
Journal of Aircraft (1983) 20  
257-261
  
12. H.A. Saberi      Analytical Model of Rotor Wake  
Aerodynamics in Ground Effect  
NASA CR 166533 December 1983
  
13. M. Nsi Mba, C. Meylan,  
C. Maresca, D. Favier      Radial Distribution Circulation of  
a Rotor in Hover Measured by Laser  
Velocimeter  
Paper No. 12 Tenth European  
Rotorcraft Forum The Hague  
Netherlands August 1984
  
14. O. Rand and A. Rosen      An Unsteady Prescribed Wake Model  
of the Aerodynamic Behaviour of a  
Helicopter Rotor Having Curved  
Blades  
TAE Report No. 544 November 1985  
See also: A. Rosen and O. Rand  
A Model of a Curved Helicopter  
Blade in Forward Flight  
to appear in Vertica

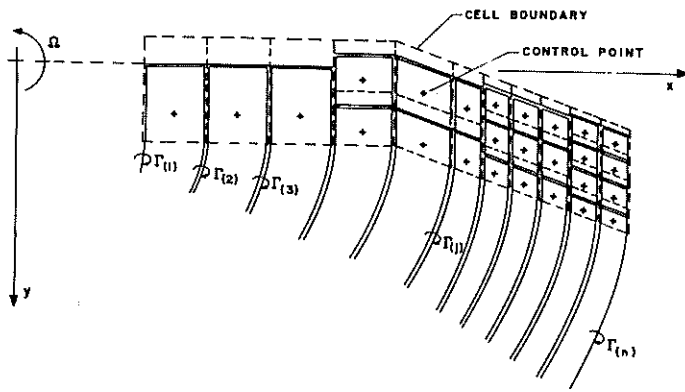


Fig. 1 - A vortex lattice model of a blade

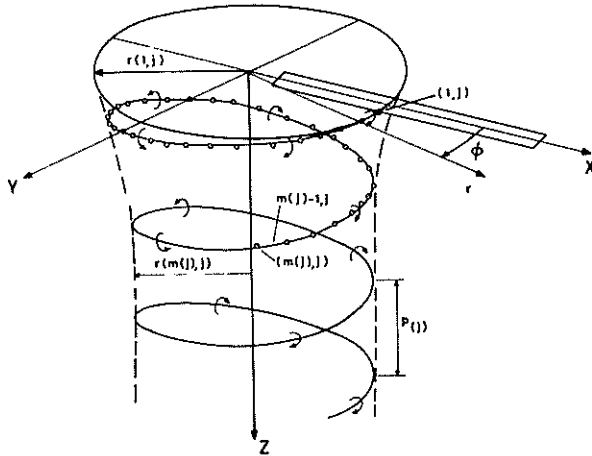


Fig. 2 - A typical vortex filament

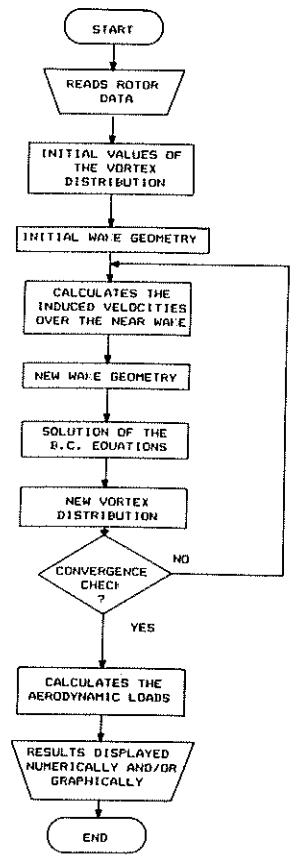


Fig. 3 - A block diagram of the solution procedure

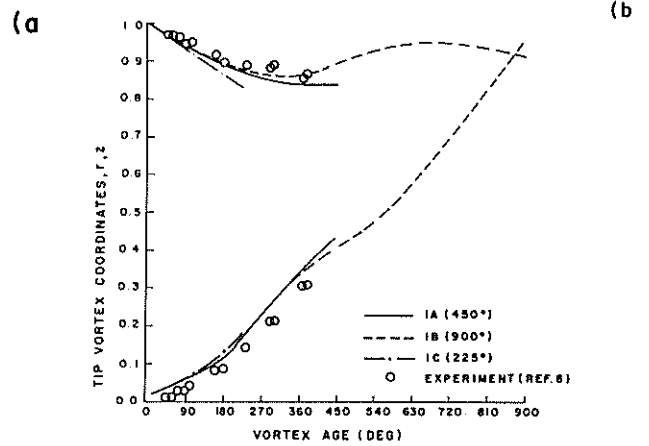
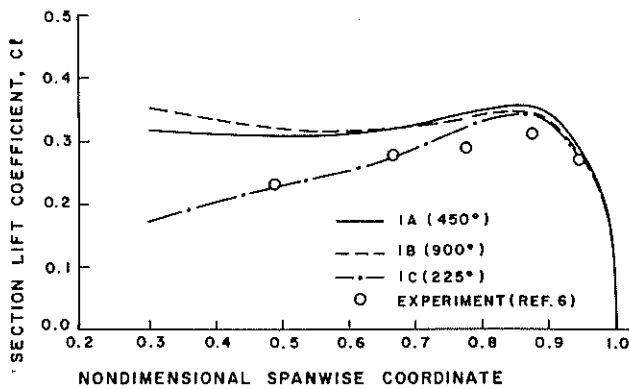


Fig. 4 - The influence of the near-wake length - rotor no. 1  
 (a) spanwise distribution of the section lift coefficient  
 (b) tip vortex geometry

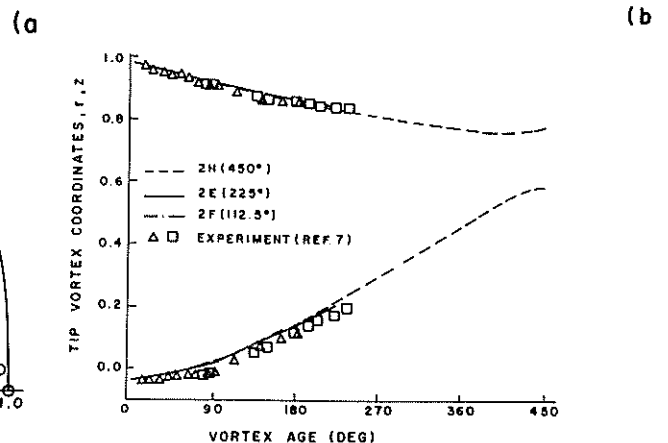
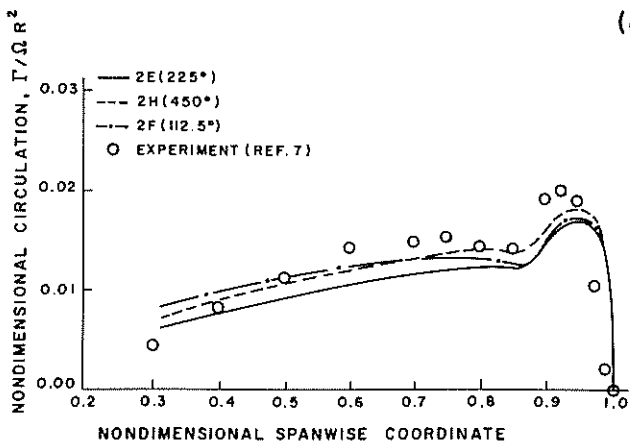


Fig. 5 - The influence of the near-wake length - rotor no. 2  
 (a) spanwise distribution of the circulation  
 (b) tip vortex geometry

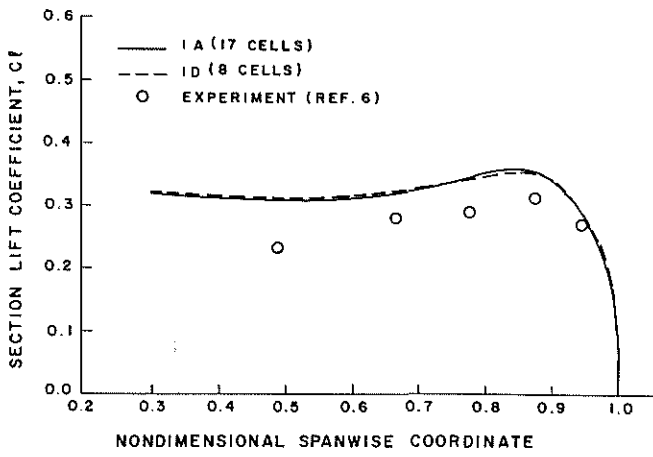


Fig. 6 - The influence of the chordwise distribution of cells - rotor no. 1

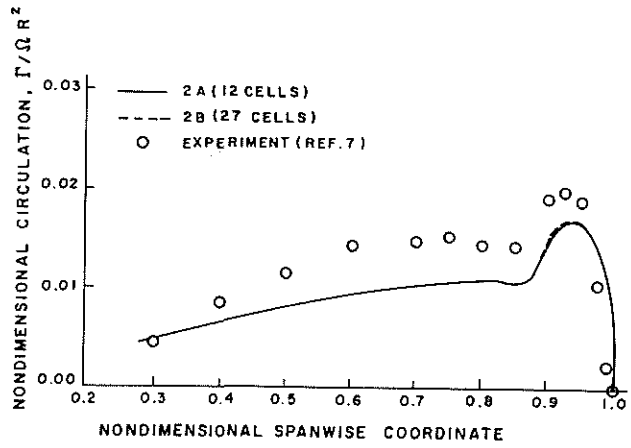


Fig. 7 - The influence of the chordwise distribution of cells - rotor no. 2

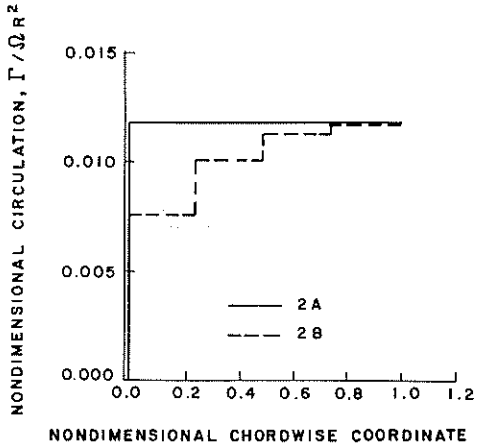


Fig. 8 - The build-up of circulation in the last column of cells - rotor no. 2

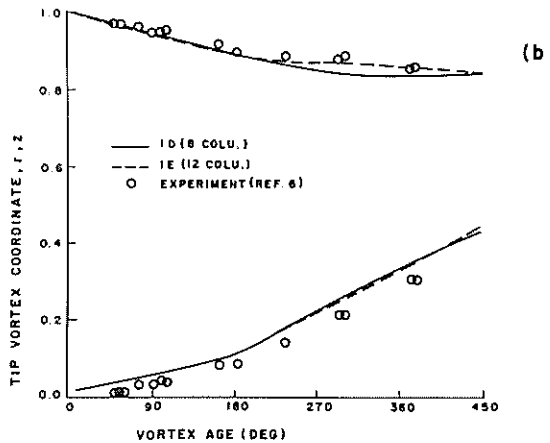
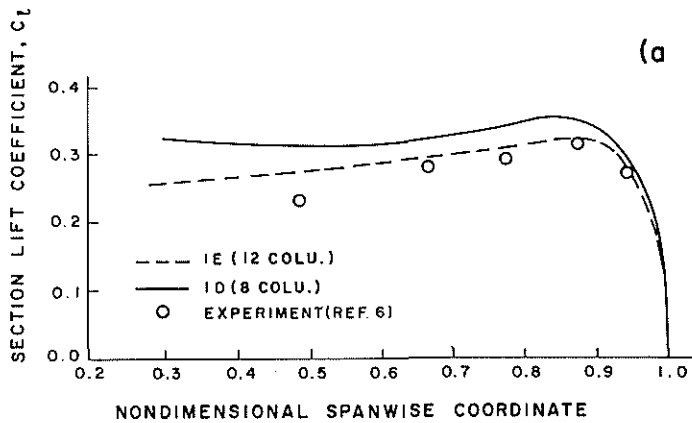


Fig. 9 - The influence of the number of columns of cells - rotor no. 1  
(a) spanwise distribution of the section lift coefficient  
(b) tip vortex geometry

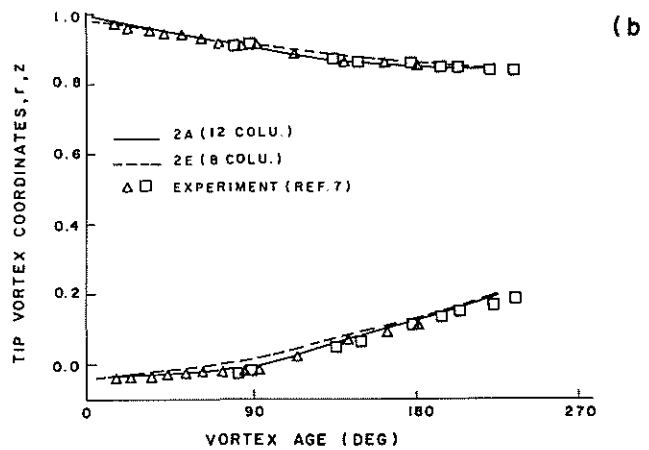
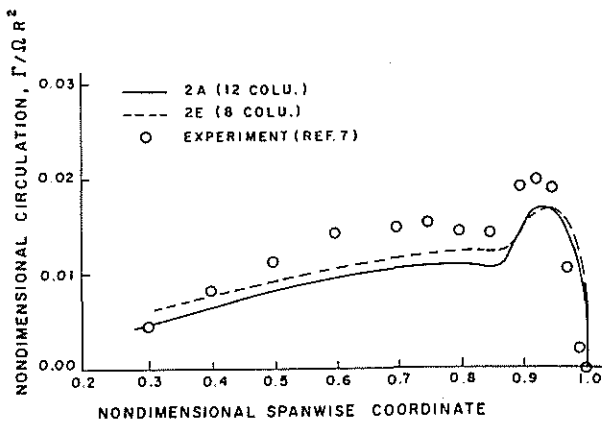


Fig. 10 - The influence of the number of columns of cells - rotor no. 2  
(a) spanwise distribution of the circulation  
(b) tip vortex geometry

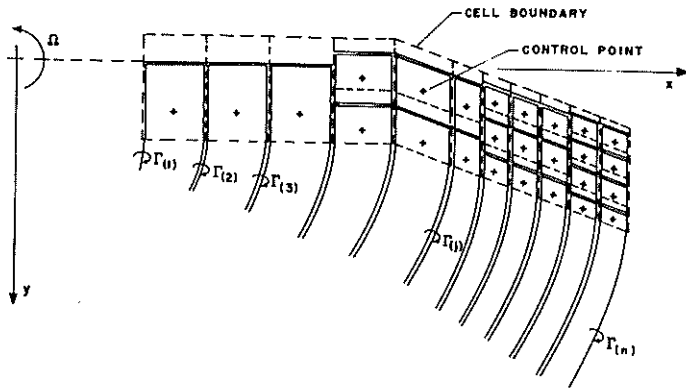


Fig. 1 - A vortex lattice model of a blade

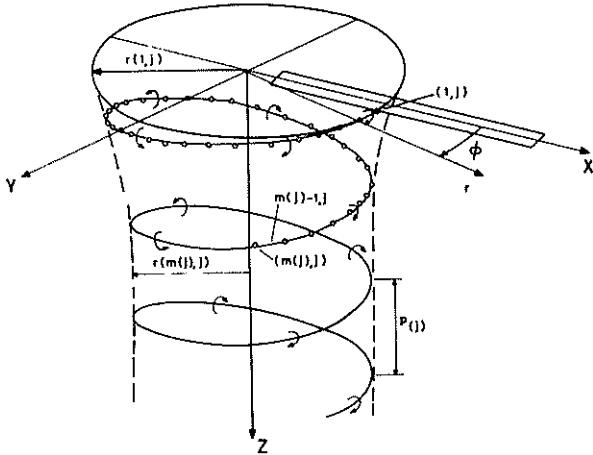


Fig. 2 - A typical vortex filament

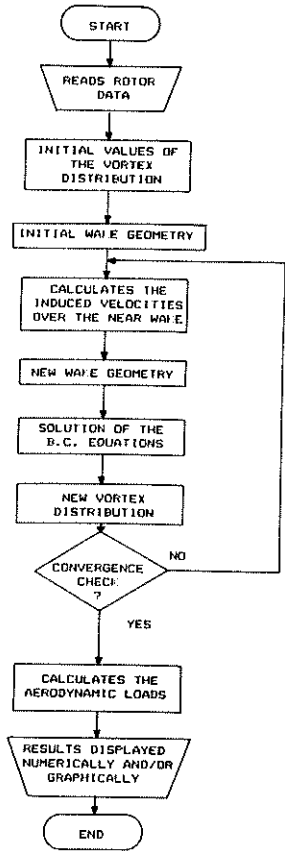


Fig. 3 - A block diagram of the solution procedure

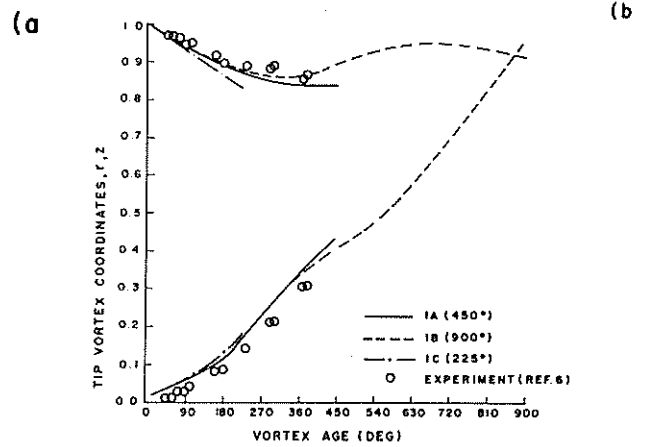
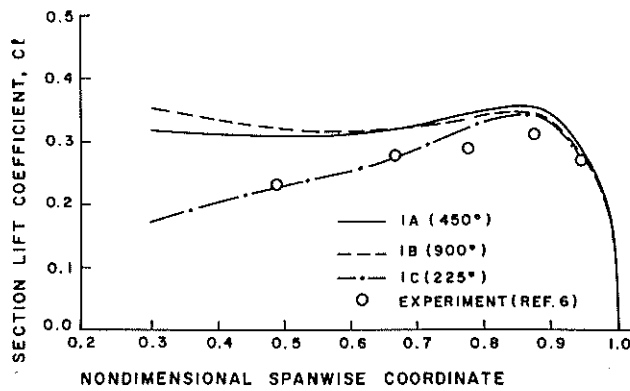


Fig. 4 - The influence of the near-wake length - rotor no. 1  
(a) spanwise distribution of the section lift coefficient  
(b) tip vortex geometry

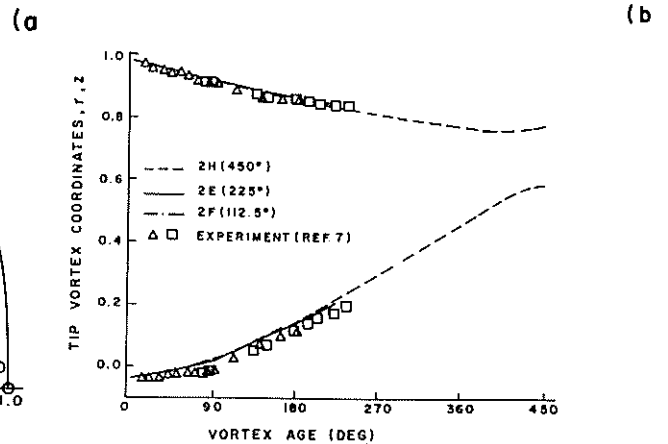
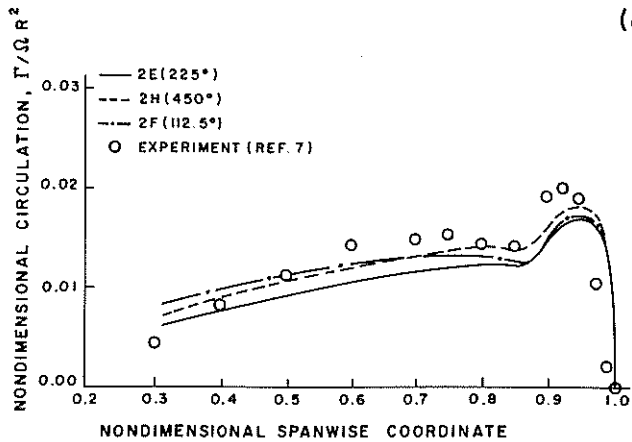


Fig. 5 - The influence of the near-wake length - rotor no. 2  
(a) spanwise distribution of the circulation  
(b) tip vortex geometry

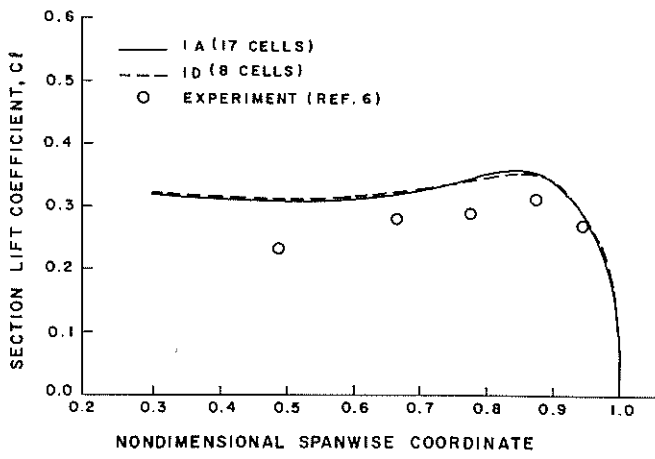


Fig. 6 - The influence of the chordwise distribution of cells - rotor no. 1

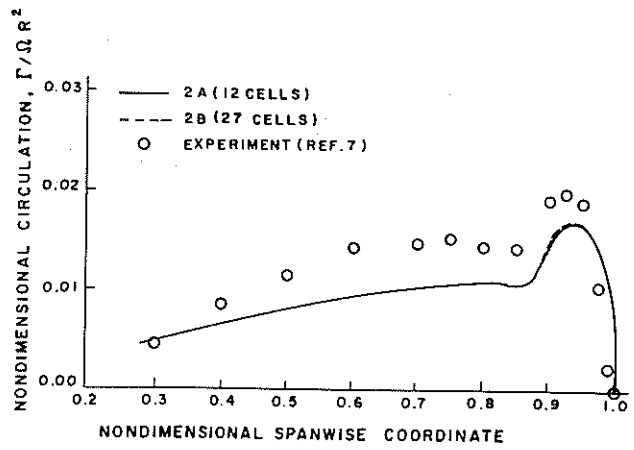


Fig. 7 - The influence of the chordwise distribution of cells - rotor no. 2

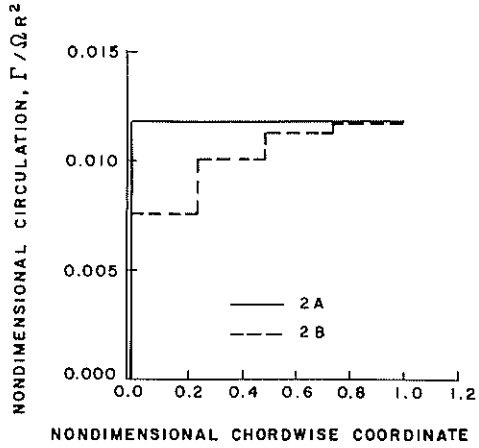


Fig. 8 - The build-up of circulation in the last column of cells - rotor no. 2

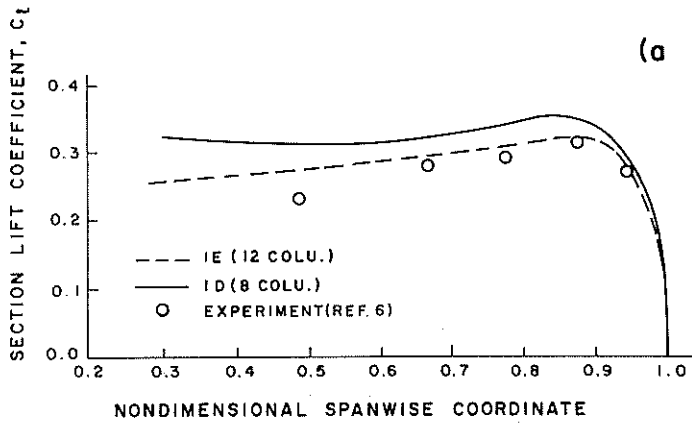
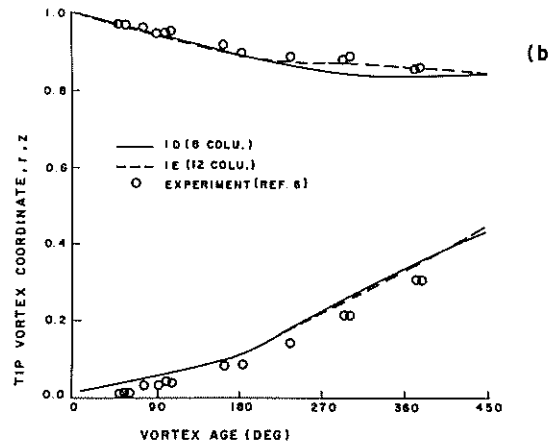


Fig. 9 - The influence of the number of columns of cells - rotor no. 1  
(a) spanwise distribution of the section lift coefficient



(b) tip vortex geometry

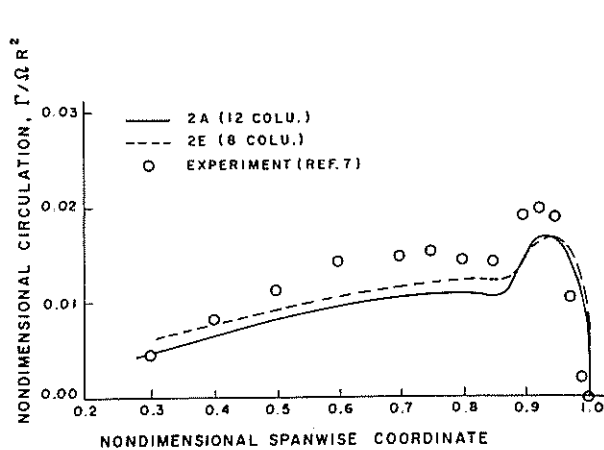
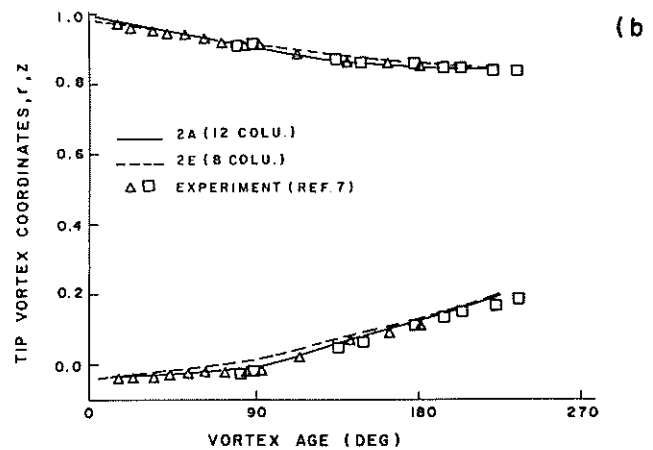


Fig. 10 - The influence of the number of columns of cells - rotor no. 2  
(a) spanwise distribution of the circulation



(b) tip vortex geometry

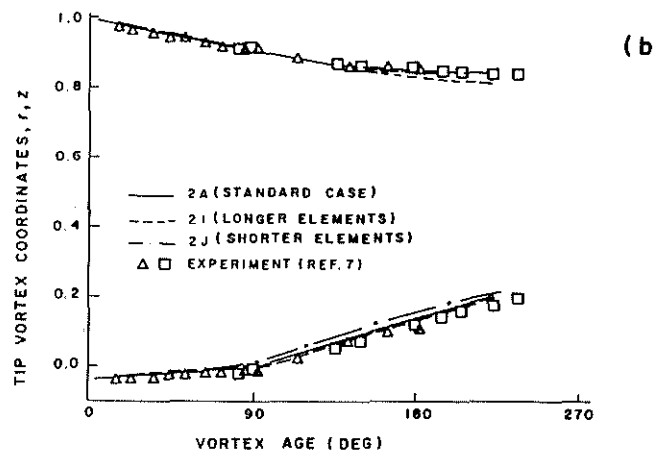
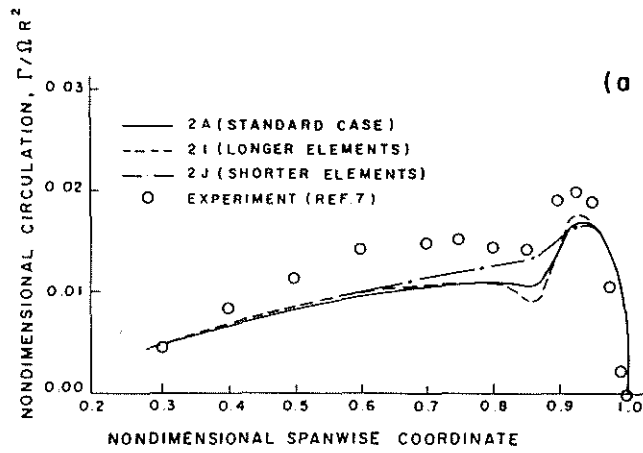


Fig. 11 - The influence of the length of the vortex elements in the near wake - rotor no. 2. (a) spanwise distribution of the circulation. (b) tip vortex geometry

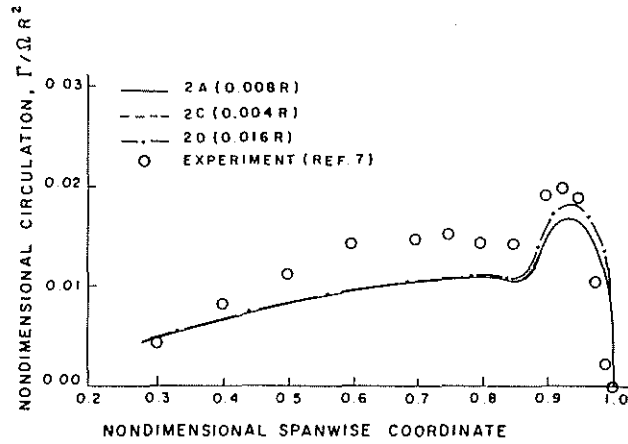


Fig. 12 - The influence of the vortex core size - rotor no. 2

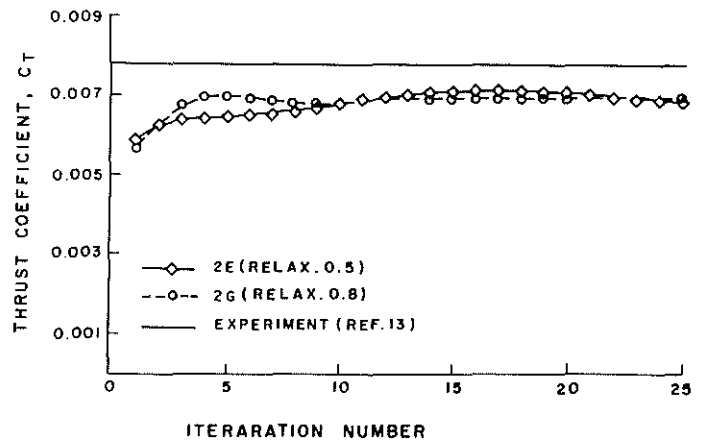


Fig. 13 - The influence of the relaxation factor on the convergence - rotor no. 2

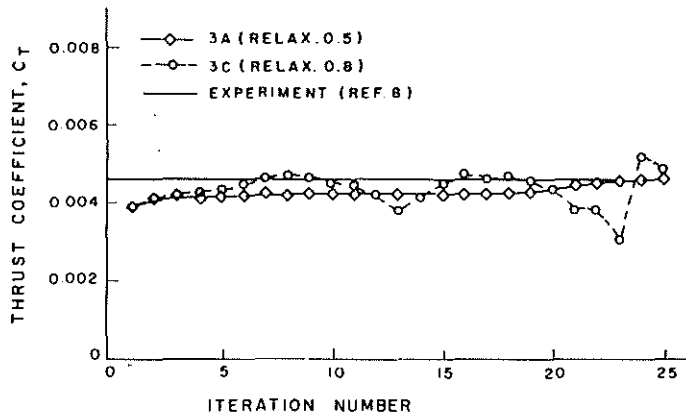


Fig. 14 - The influence of the relaxation factor on the convergence - rotor no. 3

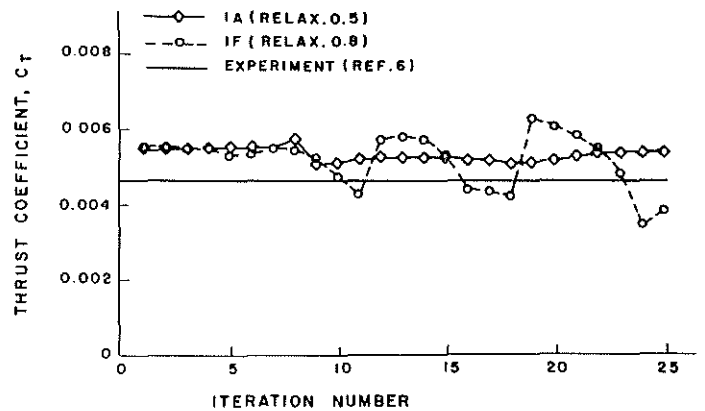


Fig. 15 - The influence of the relaxation factor on the convergence - rotor no. 1

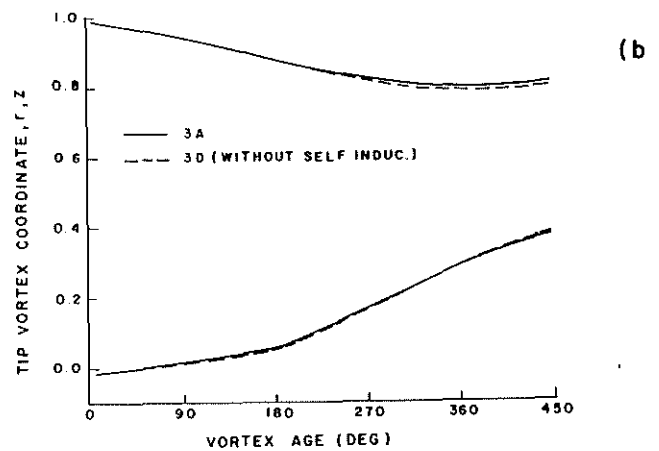
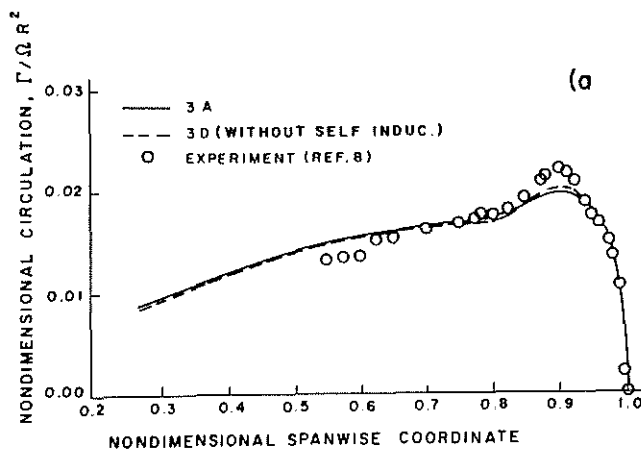


Fig. 16 - The influence of self induction correction - rotor no. 3 (a) spanwise distribution of the circulation (b) tip vortex geometry

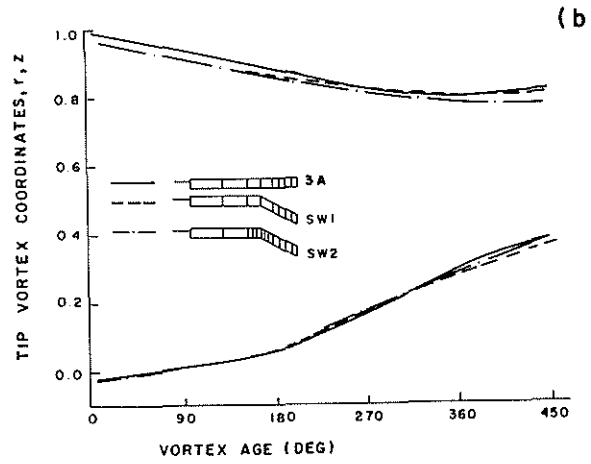
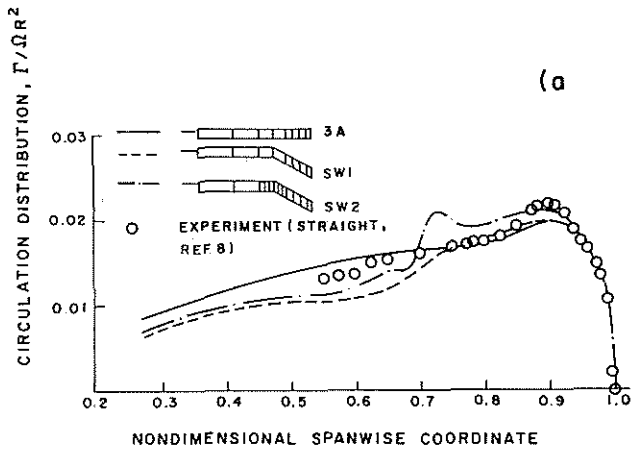


Fig. 17 - The influence of sweep back on the aerodynamic behavior  
 (a) spanwise distribution of the circulation  
 (b) tip vortex geometry

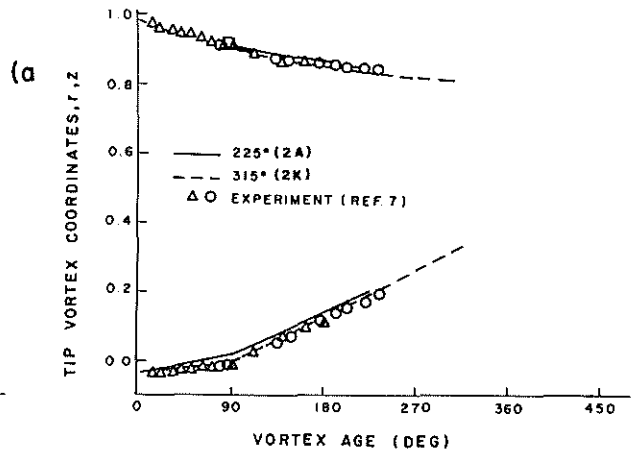
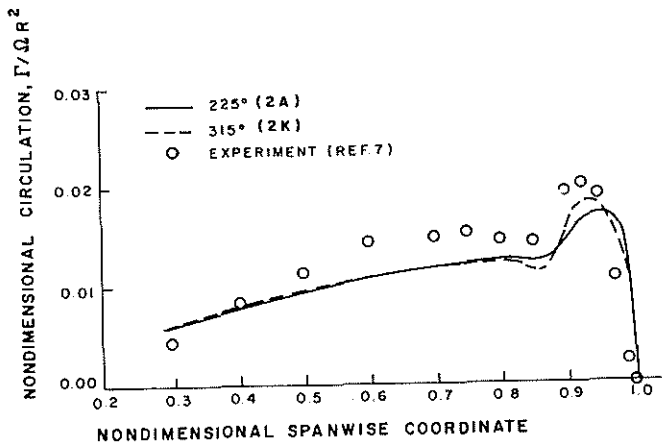


Fig. 18 - Results for an "optimal" configuration of rotor no. 2  
 (a) spanwise distribution of the circulation  
 (b) tip vortex geometry